

Calcineurin regulates endothelial barrier function by interaction with and dephosphorylation of myosin phosphatase

Bernadett Kolozsvári¹, Éva Bakó¹, Bálint Bécsi^{1,2}, Andrea Kiss¹, Ágnes Czikora³, Attila Tóth³, György Vámosi⁴, Pál Gergely¹, and Ferenc Erdődi^{1,2*}

¹Department of Medical Chemistry, Medical and Health Science Center, University of Debrecen, Nagyerdei krt 98, Debrecen H-4032, Hungary; ²Cell Biology and Signaling Research Group of the Hungarian Academy of Sciences, University of Debrecen, Debrecen H-4032, Hungary; ³Institute of Cardiology, Division of Clinical Physiology, University of Debrecen, Debrecen H-4032, Hungary; and ⁴Department of Biophysics and Cell Biology, Medical and Health Science Center, University of Debrecen, Debrecen H-4032, Hungary

Received 6 February 2012; revised 11 July 2012; accepted 1 August 2012; online publish-ahead-of-print 6 August 2012

Time for primary review: 21 days

| | |
|----------------------------|---|
| Aims | Calcineurin (CN) influences myosin phosphorylation and alters endothelial barrier function; however, the molecular mechanism is still obscure. Here we examine whether CN controls myosin phosphorylation via mediating the phosphorylation state of Thr696 in myosin phosphatase (MP) target subunit 1 (MYPT1), the phosphorylation site inhibitory to the catalytic activity of MP. |
| Methods and results | Exposure of bovine or human pulmonary artery endothelial cells (BPAECs or HPAECs) to the CN inhibitor cyclosporin A (CsA) induces a rise in intracellular Ca ²⁺ and increases the phosphorylation level of cofilin ^{Ser3} and MYPT1 ^{Thr696} in a Ca ²⁺ - and Rho-kinase-dependent manner. An active catalytic fragment of CN overexpressed in tsA201 cells decreases endogenous MYPT-phospho-Thr696 (MYPT1 ^{pThr696}) levels. Purified CN dephosphorylates ³² P-labelled MYPT1, suggesting direct action of CN on this substrate. Interaction of MYPT1 with CN is revealed by MYPT1 pull-down experiments and colocalization in both BPAECs and HPAECs as well as by surface plasmon resonance (SPR)-based binding studies. Stabilization of the MYPT1–CN complex occurs via the MYPT1 ^{300PLIEST305} sequence similar to the CN substrate-docking PxlIT-motif. Thrombin induces a transient increase of MYPT1 ^{pThr696} in BPAECs, whereas its combination with CsA results in maintained phosphorylation levels of both MYPT1 ^{pThr696} and myosin. These phosphorylation events might correlate with changes in endothelial permeability since CsA slows down the recovery from the thrombin-induced decrease of the transendothelial electrical resistance of the BPAEC monolayer. |
| Conclusion | CN may improve endothelial barrier function via inducing dephosphorylation of cofilin ^{pSer3} and by interaction with MYPT1 and activating MP through MYPT1 ^{pThr696} dephosphorylation, thereby affecting actin polymerization and decreasing myosin phosphorylation. |
| Keywords | Myosin phosphatase • Calcineurin (protein phosphatase-2B) • Myosin phosphatase target subunit 1 (MYPT1) • Endothelial barrier function • Transendothelial electrical resistance |

1. Introduction

An important function of vascular endothelial cells (ECs) is to maintain a selective barrier, thereby controlling the exchange of molecules and cells across the wall of blood vessels.¹ Physiological and/or pathological stimuli (e.g. inflammation, allergy, physical injury) may change the integrity of ECs, leading to the formation of gaps between the cells, thus compromising barrier function and

increasing vessel permeability. The cytoskeletal and intercellular junction proteins of ECs play an important role in the regulation of barrier integrity, and their physiological functions are often mediated by phosphorylation on Ser/Thr/Tyr residues.^{2,3} These findings directed our attention to uncover the types of protein kinases and phosphatases implicated in the phosphorylation of key endothelial proteins involved in the mediation of endothelial permeability.⁴

* Corresponding author. Tel: +36 52 412345; fax: +36 52 412566, Email: erdodi@med.unideb.hu

Actomyosin-based contractility of ECs is involved in the regulation of cell shape and stress fibre formation, which are major factors in the development of intercellular gaps during decreased barrier integrity.⁵ The contraction of ECs is elicited by increase in intracellular Ca^{2+} [Ca^{2+}]_i and in the phosphorylation of the 20 kDa regulatory light chain of non-muscle myosin II (MLC20). The latter is balanced by the actual activity ratio of MLC20 kinases (MLCKs) and myosin phosphatase (MP).⁶

MP consists of the δ isoform of protein phosphatase-1 (PP1) catalytic subunit (PP1c δ), PP1c δ -associated 130–133 kDa regulatory protein termed myosin phosphatase target subunit 1 (MYPT1), and a 20 kDa protein bound to the C-terminal region of MYPT1.⁷ It is regulated via the RhoA/RhoA-activated kinase (ROK) pathway since ROK phosphorylates Thr696 and Thr853 in MYPT1, resulting in the inhibition of phosphatase activity.^{8,9} MP inhibition could also occur by a 17 kDa protein termed CPI-17, which is activated via phosphorylation at Thr38 by protein kinase C or ROK.¹⁰ CPI-17 is expressed in ECs and involved in histamine- and thrombin-induced barrier dysfunction¹¹ as well as in antagonizing thrombin-induced MP inactivation by cAMP/PKA.¹² The level of phosphorylated MYPT1-Thr696 (MYPT1^{PThr696}) reflects the activity status of MP and it is correlated with the extent of MLC20 phosphorylation and the changes in endothelial permeability.^{13–15} Thus, uncovering the physiological regulation of the phosphorylation status of MYPT1 may significantly contribute to understanding these processes. The kinases that phosphorylate MYPT1 at Thr696 are quite well characterized, whereas the phosphatases involved in dephosphorylation are much less understood. Protein phosphatase-2A (PP2A) and the Ca^{2+} -calmodulin (CaM)-dependent protein phosphatase, termed calcineurin (CN) or protein phosphatase-2B (PP2B), were considered as potential MYPT1 phosphatases acting on MYPT1^{PThr696} and MYPT1^{PThr853} as revealed by *in vitro* assays.¹⁶ CN/PP2B has been implicated in the mediation of both myosin phosphorylation¹⁷ and endothelial permeability¹⁸; however, its cellular targets are not unambiguously identified yet.

We showed recently that CN contributed to the recovery of ECs from thrombin-induced barrier dysfunction, whereas pharmacological inhibition of CN by cyclosporin A (CsA) or FK506 prolonged the contractile effect and maintained gap formation between ECs.¹⁹ The goals of the present study were to dissect the molecular mechanism by which CN may affect the contractile machinery, with special interest in the mediation of MLC20 phosphorylation by the regulation of MP. Our present data suggest that CN is directly involved in the dephosphorylation of MYPT1 at both MYPT1^{PThr696} and MYPT1^{PThr853}, and it influences the phosphorylation level of cofilin too. It is concluded that CN mediates MLC20 phosphorylation via the regulation of MP and actin filament reorganization with a concomitant effect on endothelial permeability. Moreover, dephosphorylated MYPT1 and CN form a stable interaction which may have physiological implications in localizing these proteins to important signalling complexes.

2. Methods

2.1 Materials

Materials (chemicals and vendors) are given in Supplementary material online.

2.2 Proteins and antibodies

Glutathione-S-transferase (GST)-coupled full-length MYPT1 (GST-MYPT1^{1–1004}) and a C-terminal fragment (GST-MYPT1^{667–1004})⁸ or hexahistidine (His)-tagged N-terminal MYPT1 fragments (His-MYPT1^{1–633},

His-MYPT1^{1–296}, His-MYPT1^{304–511})²⁰ were expressed in *Escherichia coli* and purified as described. PP1c and PP2Ac were purified from rabbit skeletal muscle.²¹ CN was purified from bovine brain.²² The antibodies and immunochromicals used are detailed in Supplementary material online.

2.3 Cell cultures, treatments, and transfections

Bovine pulmonary artery endothelial cells (BPAECs) from American Type Tissue Culture Collection (Rockville, MD, USA) and human pulmonary artery endothelial cells (HPAECs) from Clonetics (San Diego, CA, USA) were cultured and utilized as previously described.¹⁹ Cells were treated with effectors in serum-free medium. Cells of tsA201 were grown to 60–70% confluency and transfected with pEGFP, Δ CN-A/pEGFP, Flag-MYPT1, and CN-A α /pEGFP plasmids using jetPEI transfection reagent according to the manufacturer's instructions. Flow cytometry analysis and measurement of [Ca^{2+}]_i were carried out as given in Supplementary material online.

2.4 Immunoblotting

Proteins were resolved by sodium dodecyl sulfate-polyacrylamide gel electrophoresis (SDS-PAGE) on 10–20% acrylamide gels and blotted onto nitrocellulose membranes²³ which were exposed to the antibodies and analysed as given in Supplementary material online.

2.5 Pull-down assays

GST-MYPT1 pull-down from BPAEC lysates were performed as described previously.²⁴ Cells of tsA201 were transfected with Flag-peptide (Asp-Tyr-Lys-Asp-Asp-Asp-Asp-Lys)-coupled MYPT1 (Flag-MYPT1) or co-transfected with Flag-MYPT1 plus CN-A α /pEGFP plasmids. Flag-MYPT1 as well as its associated proteins were isolated from cell lysates on anti-Flag resin according to the manufacturer's recommendations. Resin-bound proteins were solubilized by boiling in SDS sample buffer and were subjected to western blotting using anti-MYPT1^{1–296}, anti-CN-A α , anti-PP1c δ , and anti-GFP antibodies.

2.6 Dephosphorylation of ³²P-labelled MYPT1 by CN, PP1c, and PP2Ac

GST-MYPT1 was phosphorylated by ROCK in the presence of [γ -³²P]ATP and Mg^{2+} to an extent of 1.6 mol ³²P/mol MYPT1 incorporation.²⁵ Phosphatase assays were accomplished as given in Supplementary material online.

2.7 Surface plasmon resonance

Interaction of MYPT1 with CN was analysed by SPR using a Biacore 3000 instrument. GST- and His-tagged MYPT1 proteins were immobilized on CM5 sensor chips and determination of the binding of CN or PP1c on these surfaces was performed as described.²³ Kinetic parameters and the association constant (K_a) values were extracted from the sensograms using the BIAevaluation 3.1 software.

2.8 Measurement of transendothelial electrical resistance

Transendothelial electrical resistance (TER) was measured dynamically across a confluent monolayer of BPAECs, using an electrical cell-substrate impedance sensing system (Applied Biophysics, Troy, NY, USA) as described previously.²⁶ Decreases in monolayer resistance to electrical current flow, which correlated with paracellular gap formation, were measured according to the method described.²⁷

2.9 Immunofluorescence and confocal microscopy

BPAECs and HPAECs were prepared for immunofluorescence as described¹⁹ and were imaged on an Olympus Fluoview 1000 confocal microscope (Hamburg, Germany) using a 60 \times UPLSAPO (NA 1.35) oil

immersion objective. Pearson's correlation coefficients were determined as described.²⁸

2.10 Statistical analysis

Statistical significance of differences in measured variables between control and treated samples was determined by Student's *t*-test or one-way ANOVA. Difference was considered significant at $P < 0.05$ and indicated as * $P < 0.05$, ** $P < 0.01$, or *** $P < 0.001$.

3. Results

3.1 CN dephosphorylates MYPT1 in endothelial and tsA201 cells

Pharmacological inhibition of CN by CsA in cultured BPAECs (Figure 1A) or HPAECs (Figure 1B) resulted in a marked increase (~3.5 and 2.1-fold, respectively) in MYPT1^{P^{Thr696}}, indicating that

CN was involved in the dephosphorylation of this residue. H1152, a specific ROK inhibitor, inhibited the CsA-induced increase in MYPT1^{P^{Thr696}}, suggesting the role of ROK in the phosphorylation process. CsA also increased MYPT1^{P^{Thr853}}, but to a somewhat smaller extent than that of MYPT1^{P^{Thr696}} in both BPAECs and HPAECs (see Supplementary material online, Figure S1A and B) also in an ROK-dependent manner. Changes in endogenous MYPT1^{P^{Thr696}} were also determined (Figure 1C) in tsA201 cells transfected with a plasmid coding for a pEGFP-coupled constitutively active CN-A form, in which the CaM-binding and autoinhibitory domains were truncated (Δ CN-A/pEGFP).¹⁹ The per cent changes in MYPT1^{P^{Thr696}} were estimated by densitometry of western blots and untransfected cells served as a control (100%). After overexpression of Δ CN-A/pEGFP or pEGFP alone, MYPT1^{P^{Thr696}} levels were 49 ± 9 and $142 \pm 41\%$ ($n = 3$) compared with control, respectively, implying again the role of CN in MYPT1 dephosphorylation.

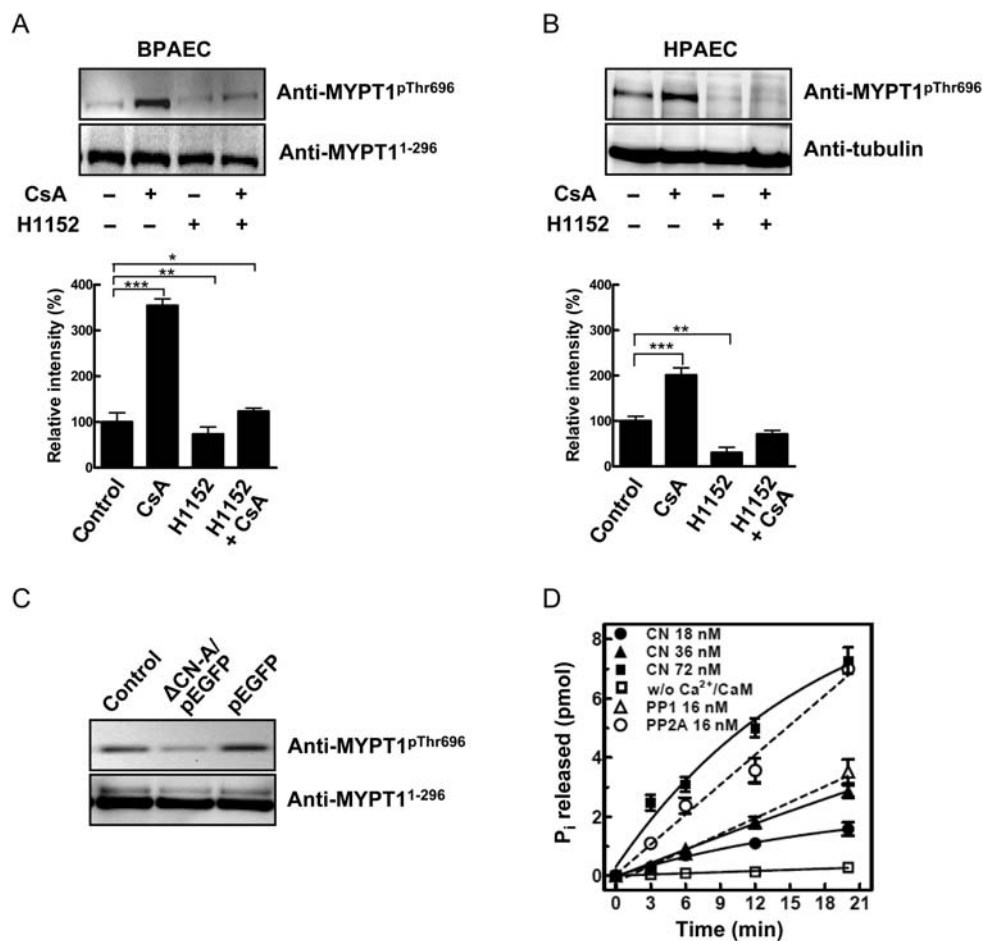


Figure 1 CN is involved in the control of the phosphorylation level of MYPT1^{Thr696}. Confluent BPAECs (A) or HPAECs (B) were incubated in the absence (control) or in the presence of 2 μ M CsA, 10 μ M H1152, or 10 μ M H1152 followed by 2 μ M CsA for 30 min. (C) Effect of overexpression of a constitutively active, truncated CN form (Δ CN-A/pEGFP) on MYPT1^{P^{Thr696}} level in tsA201 cells. Cells were lysed, boiled in SDS sample buffer, and subjected to western blot analysis using anti-MYPT1^{P^{Thr696}}, anti-MYPT1¹⁻²⁹⁶, and anti-tubulin antibodies. The results shown are representative blots of three independent experiments (upper panels). Densitometry of the MYPT1^{P^{Thr696}} bands normalized for the respective bands of MYPT1 or tubulin loading controls was carried out to quantify changes in MYPT1^{P^{Thr696}} (A and B, lower panels). (D) Dephosphorylation of ³²P-MYPT1 by CN, PP1c, and PP2Ac. The release of ³²P_i from 0.5 μ M ³²P-MYPT1 (1.6 mol phosphate/mol MYPT1) by PP1c, PP2Ac, and CN was determined at the indicated phosphatase concentrations and time intervals. CN was assayed in the absence (at 72 nM) or presence (18, 36, and 72 nM) of 0.2 mM Ca²⁺ and 40 μ g/mL CaM. The results are expressed as pmol ³²P_i released from ³²P-MYPT1 (mean \pm SEM of three independent experiments).

In *in vitro* phosphatase assays, purified CN dephosphorylated recombinant GST-MYPT1 substrate (^{32}P -labelled at Thr696 and Thr853 via phosphorylation by ROK) in a dose- and Ca^{2+} -CaM-dependent manner (Figure 1D). The kinetics of dephosphorylation were similar to those observed with PP1c and PP2Ac. These data suggested a direct action of CN on phosphorylated MYPT1.

The highly Ca^{2+} -CaM-dependent dephosphorylation of MYPT1 by CN raised a concern of how CN inhibition by CsA may result in a robust increase in MYPT1^{PThr696} in unstimulated ECs at presumably low $[\text{Ca}^{2+}]_i$ and CN activity. We examined the effect of CsA on $[\text{Ca}^{2+}]_i$ of BPAECs and found that CsA evoked an increase in $[\text{Ca}^{2+}]_i$ which was dependent on the presence of extracellular Ca^{2+} (Figure 2A). Before the addition of CsA values of 340/380 nm excitation ratio were 0.66 ± 0.01 in the presence or 0.54 ± 0.02 in the absence of extracellular Ca^{2+} , i.e. in the presence of EGTA. The CsA-induced increase in $[\text{Ca}^{2+}]_i$ was transient, reaching a maximum within 2 min (1.71 ± 0.30), then decreased, but still remained at a higher level (0.99 ± 0.16) than the initial $[\text{Ca}^{2+}]_i$ (Figure 2B) till the end of the incubation period with CsA. Increase in $[\text{Ca}^{2+}]_i$ coupled with CN activation has been implicated in inducing the dephosphorylation of cofilin-phospho-Ser-3 (cofilin^{pSer3}) via Slingshot phosphatase in HeLa cells.²⁹ Accordingly, when BPAECs or HPAECs were challenged with CsA, an increase in cofilin^{pSer3} was observed

(Figure 2C and D) in both BPAECs and HPAECs. An apparent increase in the F-actin content of HPAECs was also seen by fluorescent microscopy (see Supplementary material online, Figure S3), highlighting another consequence of CN inhibition in ECs. The necessity of elevated $[\text{Ca}^{2+}]_i$ to increase MYPT1^{PThr696} was also assessed in BPAECs. In the absence of intracellular Ca^{2+} , CsA had no effect on the level of MYPT1^{PThr696} (Figure 2E).

3.2 Interaction of MYPT1 with CN as revealed by pull-down, coexpression, and colocalization experiments

Pull-down experiments with Flag-MYPT1 and GST-MYPT1 in tsA201 and EC lysates containing endogenous CN were carried out to analyse the physiological relevance of MYPT1 and CN interaction. CN- α (Figure 3A, left panel, and see Supplementary material online, Figure S2A) and PP1c δ (Figure 3A, left) were identified as Flag-MYPT1 interacting proteins in tsA201 cells as judged by western blots. When both Flag-MYPT1 and CN- α /pEGFP were coexpressed in tsA201 cells, the coprecipitation of these proteins was also observed (see Supplementary material online, Figure S2B). Flag-MYPT1 isolated from tsA201 cells on anti-Flag resin (and freed of associated proteins) pulled down CN- α and PP1c δ from both BPAEC and HPAEC lysates

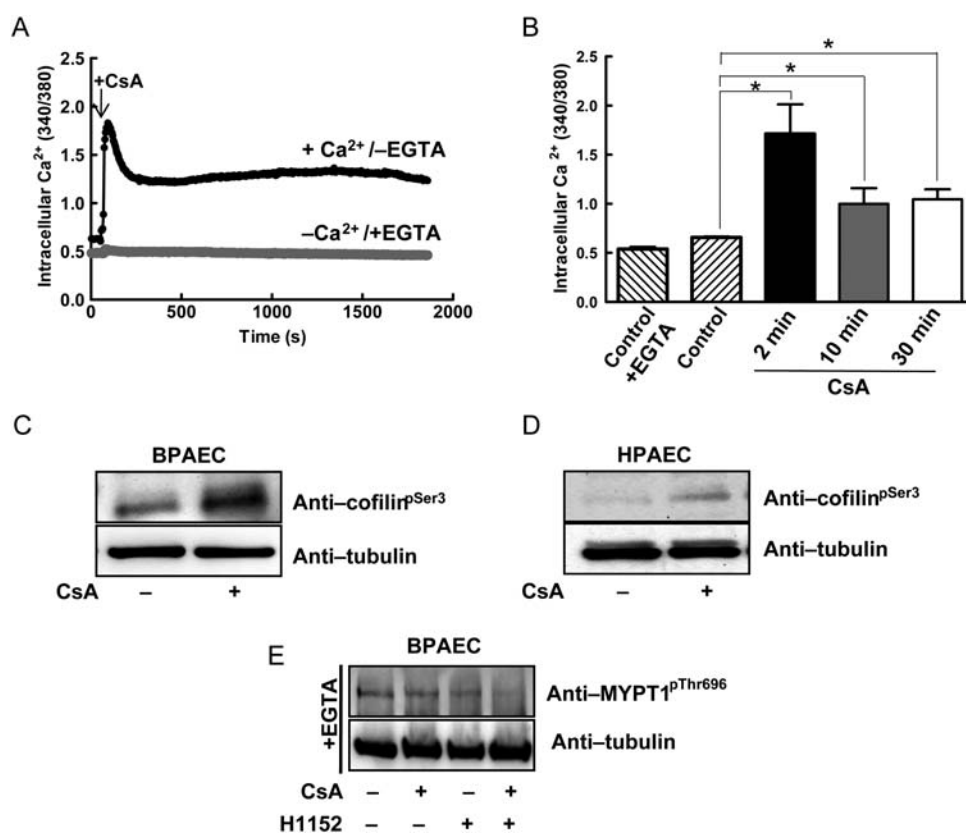


Figure 2 Effects of CsA on $[\text{Ca}^{2+}]_i$ and on the phosphorylation of cofilin^{Ser3} and MYPT1^{Thr696}. BPAECs were treated with 2 μM CsA for 30 min at room temperature. (A) Changes in $[\text{Ca}^{2+}]_i$ upon the addition of CsA were recorded with Fura-2 Ca^{2+} sensitive dye. Values for individual cells were calculated and the average response of 22–26 cells in a single representative experiment are shown in the presence (+ Ca^{2+} /–EGTA) or absence (– Ca^{2+} /+EGTA) of extracellular Ca^{2+} . (B) Bars represent the average responses (values of 340/380 nm excitation ratio) \pm SEM of 92–99 cells from four to seven independent determinations, each containing 22–26 individual cells. (C and D) Effect of CsA on the phosphorylation of cofilin^{Ser3} assessed in BPAECs (C) and HPAECs (D) by western blotting with anti-cofilin^{pSer3} antibody and anti-tubulin as loading control. (E) Effect of CsA on the phosphorylation of MYPT1^{Thr696} in BPAECs in the absence of extracellular Ca^{2+} .

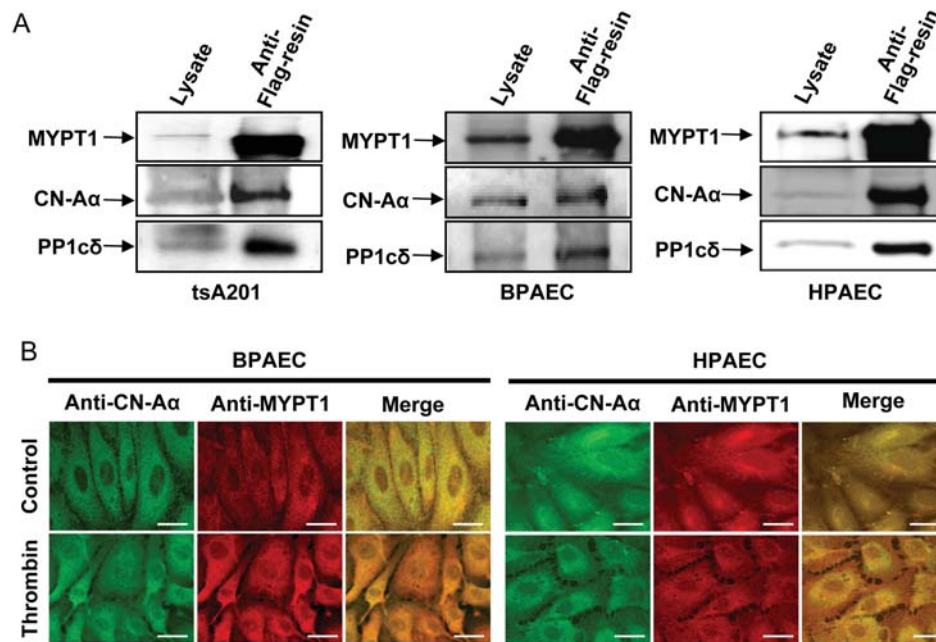


Figure 3 Interaction of MYPT1 with CN as revealed by pull-down assays and colocalization using confocal microscopy. (A) Coprecipitation of MYPT1, PP1c δ , and CN-A α from tsA201, BPAEC, and HPAEC lysates in Flag-MYPT1 pull-down assays. The bound proteins were analysed by western blotting by cutting the membranes into three pieces and then exposing them to the respective antibodies. The results shown are representative blots of three independent experiments. (B) BPAECs (left panels) or HPAECs (right panels) were stained with anti-CN-A α (green, left) or monoclonal anti-MYPT1 (red, middle) antibodies as described in Supplementary material online, and the images were merged (right) to assess colocalization. Pearson's correlation coefficients (*C*-values) calculated between the pixel intensities of the green and red channels were $C = 0.72 \pm 0.09$ ($n = 21$) and $C = 0.71 \pm 0.04$ ($n = 11$) for control and thrombin-treated BPAECs, whereas $C = 0.86 \pm 0.06$ ($n = 20$) and $C = 0.75 \pm 0.08$ ($n = 17$) for control and thrombin-treated HPAECs, respectively. Scale bars: 10 μm .

(Figure 3, middle and right panels), implicating that the interaction of MYPT1 and CN occurred at the cellular level and it was not obstructed by PP1c bound to MYPT1. Non-phosphorylated GST-MYPT1 pulled down the CN-A α subunit from EC lysate (see Supplementary material online, Figure S2C), indicating that phosphorylation of MYPT1 is not necessary to the interaction.

Confocal microscopy localized both CN-A α and MYPT1 predominantly in the cytoplasm and to a lesser extent in the nucleus in BPAECs (Figure 3B, left panels) and HPAECs (Figure 3B, right panels). The appearance of merged images suggested colocalization of these proteins in both cell types, which was confirmed by the determination of the Pearson's correlation coefficients (see *C*-values in legend to Figure 3B). Thrombin treatment induced shape change and formation of gaps between the cells; however, it did not alter the extent and pattern of the colocalization of MYPT1 and CN.

3.3 Interaction of MYPT1 and CN assessed by SPR-based binding experiments

To clarify the molecular background for the formation of the CN-MYPT1 complex, binding of CN to full-length and truncated mutants of MYPT1 was determined in SPR-based experiments using purified proteins. Figure 4A shows that CN bound to the full-length GST-MYPT1¹⁻¹⁰⁰⁴ surface in a concentration range of 1–5 μM . Assuming the formation of a 1:1 complex, an association constant of $K_a = (1.86 \pm 1.37) \times 10^7 \text{ M}^{-1}$ was derived from the binding curves. In contrast, CN hardly bound to the GST-MYPT1⁶⁶⁷⁻¹⁰⁰⁴ surface, resulting in only slight and 'noisy' increase of the resonance signals

even at higher, 5–10 μM CN concentrations (Figure 4B), implying that the C-terminal region of MYPT1 is not a major determinant in the interaction. In contrast, the mutant representing the N-terminal half of MYPT1 (His-MYPT1¹⁻⁶³³) formed a stable complex with CN ($K_a = (1.06 \pm 0.04) \times 10^7 \text{ M}^{-1}$) similar to that of the full-length MYPT1¹⁻¹⁰⁰⁴ (Figure 4C). However, the association and dissociation kinetics appeared to be distinct, which may indicate different availability of the binding sites in these two proteins and/or reflect differences in the immobilization techniques. The binding of CN to His-MYPT1¹⁻²⁹⁶ (Figure 4D) or His-MYPT1³⁰⁴⁻⁵¹¹ (Figure 4E) resulted in less stable complexes with association constants of $K_a = (3.14 \pm 1.06) \times 10^4 \text{ M}^{-1}$ and $K_a = (1.15 \pm 0.52) \times 10^5 \text{ M}^{-1}$, respectively.

Possible competition between PP1c and CN was assessed since PP1c was also shown to bind to the N-terminal MYPT1 region. Figure 4F shows that the response U obtained by injecting PP1c or CN alone until saturation were added up when the two proteins were applied in combination. Furthermore, CN was able to bind to the MYPT1 surface saturated with PP1c (Figure 4G), confirming that the binding of PP1c and CN to MYPT1 was not mutually exclusive.

3.4 Inhibition of CN by CsA sustains MYPT1 and myosin phosphorylation upon thrombin treatment accompanied by increased endothelial permeability

It was established that during thrombin treatment of ECs, transient phosphorylation of MLC20 occurs, which is coupled with transient

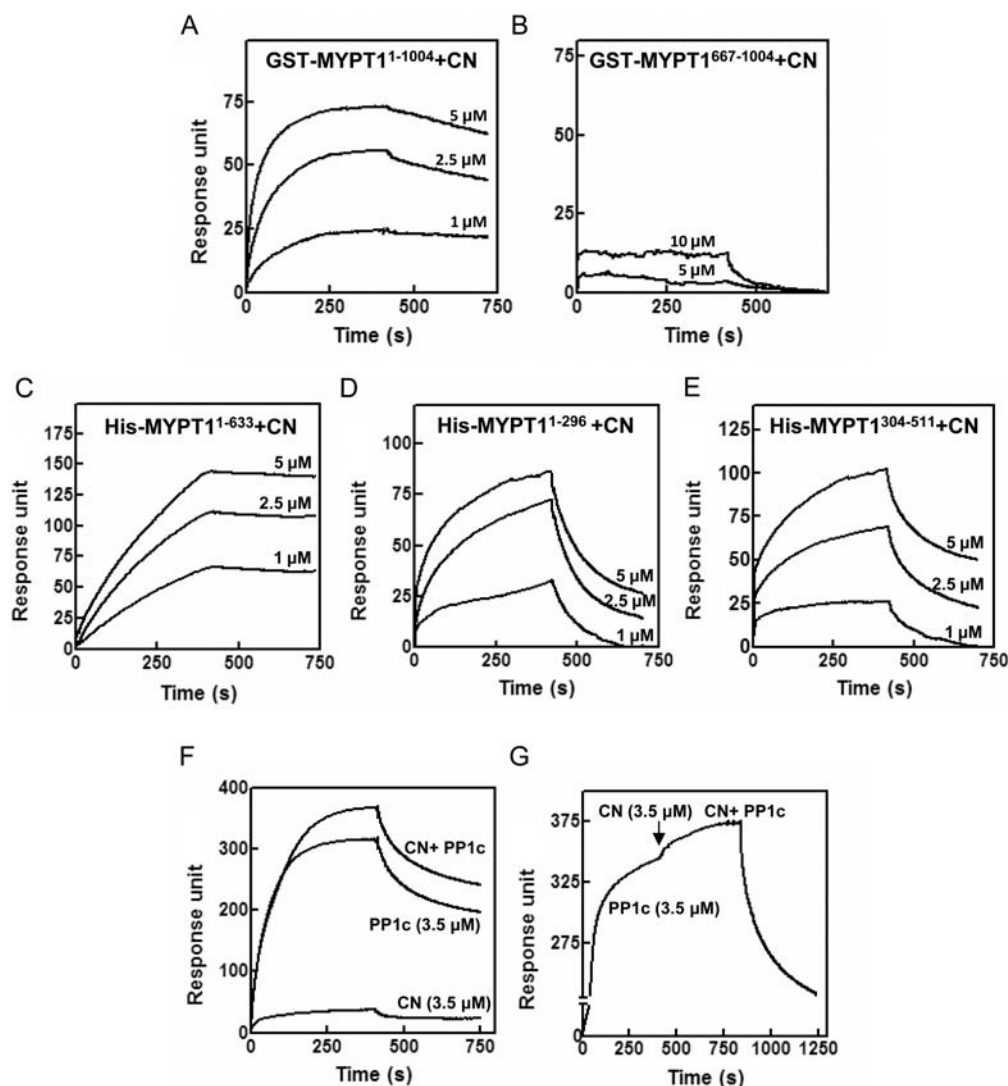


Figure 4 Characterization of the interaction between CN and MYPT1 by SPR-based binding assays. Full-length GST-MYPT1¹⁻¹⁰⁰⁴ (A, F, and G), GST-MYPT1⁶⁶⁷⁻¹⁰⁰⁴ C-terminal fragment (B) and His-MYPT1¹⁻⁶³³ (C), His-MYPT1¹⁻²⁹⁶ (D), and His-MYPT1³⁰⁴⁻⁵¹¹ (E) N-terminal fragments were immobilized on CM5 chips coupled with anti-GST (A, B, F, and G) or via direct amine coupling (C, D, and E). CN (A–G) or PP1cδ (F and G), or PP1c plus CN (F and G) was injected over the surfaces at concentrations indicated on the sensograms. Sensograms were obtained using Biacore 3000. Representative sensograms of two to three independent experiments with similar results are shown.

inactivation of MP.³⁰ Changes in MYPT1^{Thr696} following thrombin stimulation were also transient, peaking at 1 min and declining approximately to the initial level at 10 min (Figure 5A). In contrast, when BPAECs were pretreated with CsA there was a marked increase in MYPT1^{PThr696} before the addition of thrombin. This MYPT1^{PThr696} level decreased significantly (to ~75% of the maximal value) upon the addition of thrombin, but it still remained sustained at this relatively high level (Figure 5A, middle and lower panel). The most prominent difference between MYPT1^{PThr696} levels measured in the absence and presence of CsA upon the addition of thrombin was observed at 10 min. Therefore, we assessed phosphorylated MLC20-Ser19 (MLC20^{pSer19}) in BPAECs in the absence and presence of CsA after 10 min after thrombin treatment. CsA or thrombin alone slightly increased MLC20^{pSer19}, whereas a more significant increase occurred when thrombin was applied after CsA pretreatment (Figure 5B). Similar patterns were observed in

the changes of MLC20^{pSer19} in BPAECs by fluorescent staining (Figure 5C, left panel) following the above treatments. Quantification of MLC20^{pSer19} in the fluorescently labelled samples of BPAECs by flow cytometry analysis (Figure 5D) was reminiscent of the changes obtained by the densitometry of western blots (Figure 5B). The appearance of actin filaments was also altered (Figure 5C, middle panel). In the presence of CsA or thrombin, the shape of the cells changed and the amount of the stress fibres increased, whereas the combined application of CsA and thrombin resulted in the local enrichment of MLC20^{pSer19} and its colocalization with the cortical actin filaments.

Changes in the phosphorylation level of myosin are often reflected in altered endothelial barrier function. TER of BPAEC monolayers was determined by applying the same treatments as in the cell-based assays of MYPT1 and MLC20 phosphorylation. Figure 6A shows that CsA caused a rapid, significant decrease of TER for a prolonged

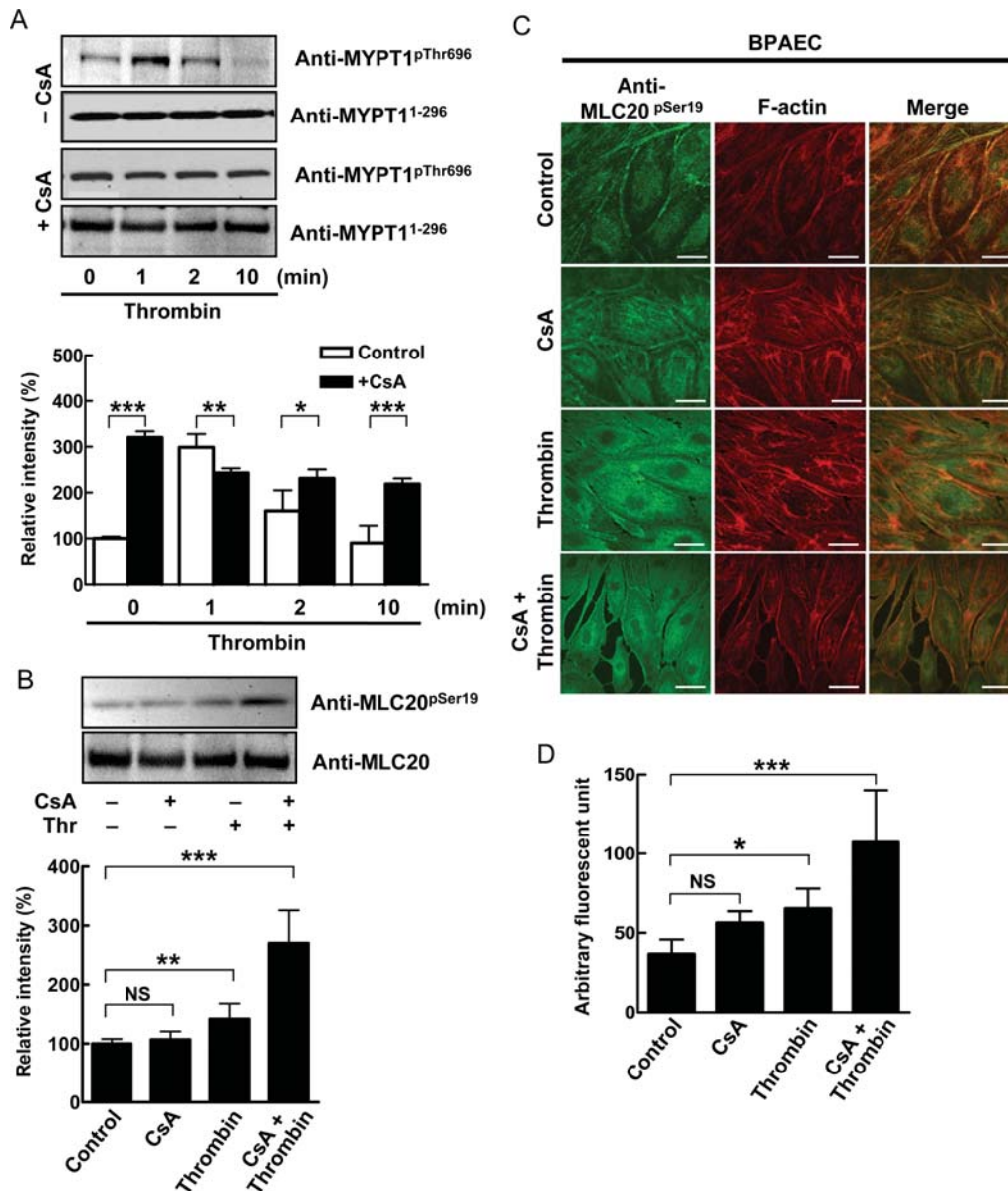


Figure 5 Effect of CN inhibition by CsA on thrombin-induced phosphorylation of MYPT1^{Thr696} and MLC20^{Ser19}. Confluent cells were pre-incubated without or with 2 μ M CsA for 30 min and then stimulated with 50 nM thrombin for different intervals. Cells were lysed and analysed by western blotting using anti-MYPT1^{pThr696} and anti-MYPT1¹⁻²⁹⁶ antibodies at 0, 1, 2, and 10 min after thrombin treatment (A), or with anti-MLC20^{pSer19} and anti-MLC20 antibodies 10 min after thrombin treatment (B). The results shown are representative blots of three independent experiments. The densitometric data are mean \pm SEM ($n = 3$). (C) BPAECs were treated with none (control), with 2 μ M CsA for 30 min, 50 nM thrombin for 10 min or 2 μ M CsA for 30 min followed by 50 nM thrombin for 10 min. Cells were stained with anti-MLC20^{pSer19} antibody and Texas Red phalloidin. Scale bars: 10 μ m. (D) Quantification of MLC^{pSer19} in fluorescent-labelled samples by flow cytometry after the indicated treatments.

period (~2 h) before recovery. Thrombin alone induced also a fast and more pronounced decrease in TER than did CsA; however, the recovery appeared to be faster and completed in 45 min. Pretreatment of BPAECs with CsA before thrombin addition did not alter the extent of decrease in TER induced by thrombin; however, a sustained decrease in TER (~1.5 h) was observed, suggesting that CsA slowed down significantly the recovery of TER. The changes in TER of BPAECs reflect alterations in endothelial permeability paralleling in part the changes in MLC20^{pSer19} observed under the same conditions.

4. Discussion

Our present work identifies CN as an MYPT1 phosphatase acting directly, and in a Ca^{2+} -CaM manner, on the PP1c inhibitory MYPT1^{pThr696} site. Dephosphorylation of MYPT1 by CN has been shown previously; however, its physiological relevance was doubted since cell lysates did not exhibit any Ca^{2+} -CaM dependent activity assayed with phospho-MYPT1 substrate.¹⁶ We provide evidence here for the direct interaction of CN with MYPT1, and the occurrence of the dephosphorylation of MYPT1 by CN at cellular level

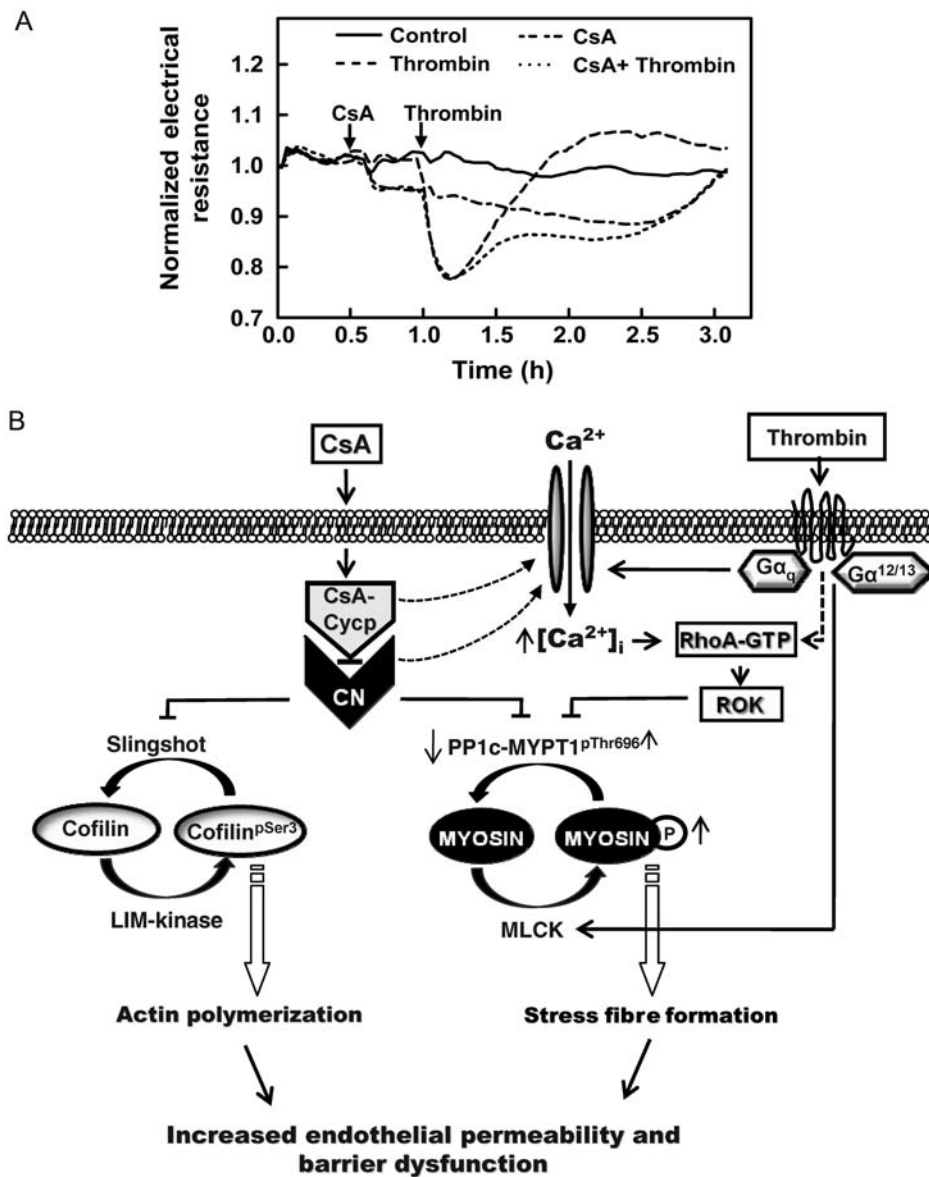


Figure 6 Influence of CsA on endothelial barrier function. (A) Effect of CsA on TER of BPAEC monolayers. Confluent monolayers of BPAECs grown on electrodes were challenged with none, 2 μ M CsA or 50 nM thrombin, or with their combination adding thrombin to the cells after 30 min pre-incubation with 2 μ M CsA (additions are indicated by arrows). TER was determined as described in Methods. Data shown are representative graphs of three experiments with similar results. (B) Depiction of the mechanisms via CsA may affect endothelial permeability in ECs (see explanations in the Discussion section).

as the CN inhibitor CsA profoundly increases the MYPT1^{pThr696} level in ECs, while the endogenous MYPT1^{pThr696} level decreases when an active truncated form of CN overexpressed in tsA201 cells. CsA induces a transient but partially maintained rise in $[Ca^{2+}]_i$ dependent upon the presence of extracellular Ca^{2+} implicating plasma membrane Ca^{2+} -channel(s) in this process (Figure 6B). The precise mechanism of this Ca^{2+} influx with respect to the involvement of the type of channel(s) as well as the role of CsA-cyclophilin complex and/or its inhibitory influence on CN requires further investigations. The CsA-induced $[Ca^{2+}]_i$ transient is a prerequisite of the increase in MYPT1^{pThr696} as it is not observed in the absence of extracellular Ca^{2+} . The rise in $[Ca^{2+}]_i$ may also increase MYPT1^{pThr696} by the

activation of ROK, since it was shown³¹ that increasing $[Ca^{2+}]_i$ is coupled with the enhancement of active RhoA (RhoA-GTP). Nevertheless, this enhanced $[Ca^{2+}]_i$ does not seem to activate MLCKs to an extent that would significantly increase MLC20^{pSer19}. On the other hand, phosphorylation of cofilin^{ser3}, an actin-depolymerizing factor, is elevated significantly in both BPAECs and HPAECs upon CsA treatment. Previous studies have shown²⁹ that an increase in $[Ca^{2+}]_i$ coupled with CN activation results in dephosphorylation and activation of Slingshot, a major cofilin^{pSer3} phosphatase, thereby lowering cofilin^{pSer3}. Elevated $[Ca^{2+}]_i$ may also increase ROK activity, which activates LIM-kinase (a cofilin kinase), thus it contributes to enhancing cofilin^{pSer3}. This elevation in cofilin^{pSer3} is further favoured by

CsA-induced CN inhibition preventing the activation of Slingshot, thus suppressing dephosphorylation. Cofilin^{pSer3} has suppressed actin-depolarizing activity; therefore, a rise in cofilin^{pSer3} may contribute to increased F-actin content and actin-filament reorganization in ECs.

The level of MYPT1^{pThr696} is a key factor in the activity status of MP and it controls MLC20 phosphorylation. CN was shown to associate with the cytoskeletal (myosin-rich) fraction of ECs¹⁷ and was phosphorylated and activated upon thrombin stimulation, resulting in the dephosphorylation of EC proteins. In contrast, in the presence of CN inhibitors, EC protein dephosphorylation including MLC20^{pSer19} was attenuated. Our results support a mechanism in which CN counterbalances the phosphorylation of the inhibitory site(s) in MYPT1 keeping MP in an active state, thereby decreasing MLC20^{pSer19}. Thrombin triggers a rise in [Ca²⁺]_i, which activates both MLCKs and CN, resulting in transient MLC20 phosphorylation and MP inhibition.³⁰ Our present data imply that the transient MP inhibition is coupled with a transient increase in MYPT1^{pThr696} (Figure 5). The role of CN in mediating MYPT1^{pThr696} dephosphorylation during thrombin stimulation is confirmed by the findings that pretreatment of ECs with CsA results in partially sustained phosphorylation of both MYPT1^{pThr696} and MLC20^{pSer19}. The role of PP1c and PP2Ac in MYPT1^{pThr696} dephosphorylation is also shown by *in vitro* phosphatase assays, but in cells they may act in holoenzyme forms, which are still not identified. Nevertheless, PP2A have been implicated in MYPT1 dephosphorylation, since PP2A-specific inhibition using cell-permeable phosphatase inhibitory toxins (okadaic acid and calyculin-A) profoundly enhanced both MYPT1^{pThr696} and MYPT1^{pThr853} in HepG2³² and THP-1 cells.²³ These 'CsA insensitive' PP2A (and PP1) enzymes may have a role in the partial decrease of MYPT1^{pThr696} during CsA plus thrombin treatment with a concomitant effect on MLC20^{pSer19}.

It was shown that CN inhibitors (CsA, FK506, dexamethasone) influence EC permeability. FK506 alone did not alter TER, but it prevented the reversal of thrombin-induced decrease in resistance, whereas PP1 and PP2A inhibitors were without effect.¹⁸ The effect of FK506 was attributed to a CN-inhibition-dependent increase in the phosphorylation of protein kinase C α . Inhibition of CN by dexamethasone also increased endothelial permeability and it was due to enhanced MLC20 phosphorylation.¹⁷ Our results suggest that CN inhibition by CsA decreases TER in BPAECs to a significant extent without a profound change in MLC20 phosphorylation. We hypothesize that this change in TER by CsA is due to an increase in cofilin^{pSer3}, resulting in enhanced actin polymerization with subsequent alterations in EC cell shape and permeability. CsA treatment also slows down the recovery of decreased TER induced by thrombin and this effect appears to parallel the sustained level of MYPT1^{pThr696} and MLC20^{pSer19}. Our data imply that CN inhibition by CsA exerts both MLC20 phosphorylation-dependent and independent effects.

Our finding that CN forms a stable complex with dephosphorylated MYPT1 indicates that the interaction between these two proteins is stronger than it would be expected for a simple enzyme-phosphosubstrate adduct. SPR-binding studies establish the essential role of the N-terminal region of MYPT1 in the interaction with CN. Accordingly, there is a CN-substrate-docking PxlIT-like motif³³ in the N-terminal region of MYPT1 (³⁰⁰PLIEST³⁰⁵), which may play an important role in the interaction with CN. Thus, MYPT1 fragments (MYPT1¹⁻²⁹⁶ and MYPT1³⁰⁴⁻⁵¹¹) lacking this motif bind to CN with lower affinity ($K_a \approx 10^4 - 10^5$) than that of the mutant representing the N-terminal half (MYPT1¹⁻⁶³³) or the full-

length (MYPT1¹⁻¹⁰⁰⁴) protein ($K_a \approx 10^7$). Nevertheless, MYPT1¹⁻²⁹⁶ and MYPT1³⁰⁴⁻⁵¹¹ still exhibit significant binding to CN, suggesting that besides the PxlIT-like docking motif further regions within these fragments are also involved in forming a stable MYPT1-CN complex. PP1c binds also to the N-terminal regions of MYPT1,³⁴ but the major docking site for PP1c in MYPT1 (³⁵KVKF³⁸) is different from that of CN (³⁰⁰PLIEST³⁰⁵). Further competitive binding sites for PP1c and CN could also be excluded as the two proteins coprecipitate with Flag-MYPT1 during pull-downs and bind independently to MYPT1 surface in SPR binding studies, suggesting that CN presumably interacts with the MP holoenzyme with the same affinity as does with MYPT1.

In summary, we identified a mechanism of how CN may modulate the phosphorylation level of MLC20 in myosin via influencing the phosphorylation state of a PP1c inhibitory site in the MYPT1 subunit of MP. It is assumed that these CN-induced changes of the phosphorylation status of MLC20 and MYPT1 are also reflected in the contractile features of ECs and in the alterations of barrier function. The relatively strong interaction formed between CN and MYPT1 (and the MP holoenzyme) may have broader physiological significance in localizing these enzymes close to their possible substrates forming functionally important signalling complexes.

Supplementary material

Supplementary material is available at *Cardiovascular Research* online.

Acknowledgements

The authors are indebted to Mrs Ella Kovács and Ágnes Németh for their excellent technical assistance. Confocal microscopy was carried out at the Molecular Cell Analysis Core Facility of the University of Debrecen.

Conflict of interest: none declared.

Funding

This work was supported by the Hungarian Scientific Research Fund (OTKA K68416 to F.E., CNK80709 to P.G., and K77600 to G.V.) and by the New Hungary Development Plan co-financed by the European Social Fund (TÁMOP 4.2.2.-08/1-2008-0019 DERMINOVA; TÁMOP-4.2.1./B-09/1/KONV-2010-0007; TÁMOP-4.2.2/B-10/1-2010-0024).

References

1. Mehta D, Malik AB. Signaling mechanisms regulating endothelial permeability. *Physiol Rev* 2006;**86**:279–367.
2. Bogatcheva NV, Verin AD. The role of cytoskeleton in the regulation of vascular endothelial barrier function. *Microvasc Res* 2008;**76**:202–207.
3. Weis SM. Vascular permeability in cardiovascular disease and cancer. *Curr Opin Hematol* 2008;**15**:243–249.
4. Csontos C, Kolosova I, Verin AD. Regulation of vascular endothelial cell barrier function and cytoskeleton structure by protein phosphatases of the PPP family. *Am J Physiol Lung Cell Mol Physiol* 2007;**293**:L843–L854.
5. Goeckeler ZM, Wysolmerski RB. Myosin light chain kinase-regulated endothelial cell contraction: the relationship between isometric tension, actin polymerization, and myosin phosphorylation. *J Cell Biol* 1995;**130**:613–627.
6. Somlyo AP, Somlyo AV. Ca²⁺ sensitivity of smooth muscle and nonmuscle myosin II: modulated by G proteins, kinases, and myosin phosphatase. *Physiol Rev* 2003;**83**:1325–1358.
7. Hartshorne DJ, Ito M, Erdődi F. Role of protein phosphatase type 1 in contractile functions: myosin phosphatase. *J Biol Chem* 2004;**279**:37211–37214.
8. Feng J, Ito M, Ichikawa K, Isaka N, Nishikawa M, Hartshorne DJ et al. Inhibitory phosphorylation site for Rho-associated kinase on smooth muscle myosin phosphatase. *J Biol Chem* 1999;**274**:37385–37390.

9. Murányi A, Derkach D, Erdődi F, Kiss A, Ito M, Hartshorne DJ. Phosphorylation of Thr695 and Thr850 on the myosin phosphatase target subunit: inhibitory effects and occurrence in A7r5 cells. *FEBS Lett* 2005;**579**:6611–6615.
10. Eto M. Regulation of cellular protein phosphatase-1 (PP1) by phosphorylation of the CPI-17 family, C-kinase-activated PP1 inhibitors. *J Biol Chem* 2009;**284**:35273–35277.
11. Kolosova IA, Ma SF, Adyshev DM, Wang P, Ohba M, Natarajan V et al. Role of CPI-17 in the regulation of endothelial cytoskeleton. *Am J Physiol Lung Cell Mol Physiol* 2004;**287**:L970–L980.
12. Aslam M, Hartel FV, Arshad M, Gunduz D, Abdallah Y, Sauer H et al. cAMP/PKA antagonizes thrombin-induced inactivation of endothelial myosin light chain phosphatase: role of CPI-17. *Cardiovasc Res* 2010;**87**:375–384.
13. Birukova AA, Smurova K, Birukov KG, Kaibuchi K, Garcia JG, Verin AD. Role of Rho GTPases in thrombin-induced lung vascular endothelial cells barrier dysfunction. *Microvasc Res* 2004;**67**:64–77.
14. Cho T, Jung Y, Koschinsky ML. Apolipoprotein(a), through its strong lysine-binding site in KIV(10'), mediates increased endothelial cell contraction and permeability via a Rho/Rho kinase/MYPT1-dependent pathway. *J Biol Chem* 2008;**283**:30503–30512.
15. van Nieuw Amerongen GP, Musters RJ, Eringa EC, Sipkema P, van Hinsbergh VW. Thrombin-induced endothelial barrier disruption in intact microvessels: role of RhoA/Rho kinase-myosin phosphatase axis. *Am J Physiol Cell Physiol* 2008;**294**:C1234–C1241.
16. Takizawa N, Niuro N, Ikebe M. Dephosphorylation of the two regulatory components of myosin phosphatase, MBS and CPI17. *FEBS Lett* 2002;**515**:127–132.
17. Verin AD, Cooke C, Herenyiova M, Patterson CE, Garcia JG. Role of Ca²⁺/calmodulin-dependent phosphatase 2B in thrombin-induced endothelial cell contractile responses. *Am J Physiol* 1998;**275**:L788–L799.
18. Lum H, Podolski JL, Gurnack ME, Schulz IT, Huang F, Holian O. Protein phosphatase 2B inhibitor potentiates endothelial PKC activity and barrier dysfunction. *Am J Physiol Lung Cell Mol Physiol* 2001;**281**:L546–L555.
19. Kolozsvári B, Sziogyártó Z, Bai P, Gergely P, Verin A, Garcia JG et al. Role of calcineurin in thrombin-mediated endothelial cell contraction. *Cytometry A* 2009;**75**:405–411.
20. Hirano K, Phan BC, Hartshorne DJ. Interactions of the subunits of smooth muscle myosin phosphatase. *J Biol Chem* 1997;**272**:3683–3688.
21. Kiss A, Bécsi B, Kolozsvári B, Komáromi I, Köver KE, Erdődi F. Epigallocatechin-3-gallate and penta-O-galloyl-beta-D-glucose inhibit protein phosphatase-1. *FEBS J* 2012 (in press).
22. Tallant EA, Wallace RW, Cheung WY. Purification and radioimmunoassay of calmodulin-dependent protein phosphatase from bovine brain. *Methods Enzymol* 1983;**102**:244–256.
23. Kiss A, Lontay B, Bécsi B, Márkász L, Oláh É, Gergely P et al. Myosin phosphatase interacts with and dephosphorylates the retinoblastoma protein in THP-1 leukemic cells: its inhibition is involved in the attenuation of daunorubicin-induced cell death by calyculin-A. *Cell Signal* 2008;**20**:2059–2070.
24. Lontay B, Serfőző Z, Gergely P, Ito M, Hartshorne DJ, Erdődi F. Localization of myosin phosphatase target subunit 1 in rat brain and in primary cultures of neuronal cells. *J Comp Neurol* 2004;**478**:72–87.
25. Wooldridge AA, MacDonald JA, Erdodi F, Ma C, Borman MA, Hartshorne DJ et al. Smooth muscle phosphatase is regulated in vivo by exclusion of phosphorylation of threonine 696 of MYPT1 by phosphorylation of Serine 695 in response to cyclic nucleotides. *J Biol Chem* 2004;**279**:34496–34504.
26. Schaphorst KL, Pavalko FM, Patterson CE, Garcia JG. Thrombin-mediated focal adhesion plaque reorganization in endothelium: role of protein phosphorylation. *Am J Respir Cell Mol Biol* 1997;**17**:443–455.
27. Giaever I, Keese CR. A morphological biosensor for mammalian cells. *Nature* 1993;**366**:591–592.
28. Vereb G, Matko J, Vamosi G, Ibrahim SM, Magyar E, Varga S et al. Cholesterol-dependent clustering of IL-2Ralpha and its colocalization with HLA and CD48 on T lymphoma cells suggest their functional association with lipid rafts. *Proc Natl Acad Sci USA* 2000;**97**:6013–6018.
29. Wang Y, Shibasaki F, Mizuno K. Calcium signal-induced cofilin dephosphorylation is mediated by Slingshot via calcineurin. *J Biol Chem* 2005;**280**:12683–12689.
30. Essler M, Retzer M, Bauer M, Heemskerck JW, Aepfelbacher M, Siess W. Mildly oxidized low density lipoprotein induces contraction of human endothelial cells through activation of Rho/Rho kinase and inhibition of myosin light chain phosphatase. *J Biol Chem* 1999;**274**:30361–30364.
31. Singh I, Knezevic N, Ahmed GU, Kini V, Malik AB, Mehta D. Galphaq-TRPC6-mediated Ca²⁺ entry induces RhoA activation and resultant endothelial cell shape change in response to thrombin. *J Biol Chem* 2007;**282**:7833–7843.
32. Lontay B, Kiss A, Gergely P, Hartshorne DJ, Erdődi F. Okadaic acid induces phosphorylation and translocation of myosin phosphatase target subunit 1 influencing myosin phosphorylation, stress fiber assembly and cell migration in HepG2 cells. *Cell Signal* 2005;**17**:1265–1275.
33. Roy J, Cyert MS. Cracking the phosphatase code: docking interactions determine substrate specificity. *Sci Signal* 2009;**2**:re9.
34. Tóth A, Kiss E, Herberg FW, Gergely P, Hartshorne DJ, Erdődi F. Study of the subunit interactions in myosin phosphatase by surface plasmon resonance. *Eur J Biochem* 2000;**267**:1687–1697.